time it is important to utilize the present advances to determine the extent of the negative-pressure domains for other liquids and to perform measurements of structural, dynamic, and thermodynamic properties of liquids within these domains.

REFERENCES AND NOTES

1. D. Chandler, J. D. Weeks, H. C. Andersen, *Science* **220**, 787 (1983).
2. B. J. Alder and T. E. Wainwright, *J. Chem. Phys.* **27**, 1208 (1957).
3. M. Berthelot, *Ann. Chem. (Ser. 3)* **30**, 232 (1850).
4. L. Briggs, *J. Appl. Phys.* **21**, 721 (1950).
5. M. Greenspan and C. Tschiegg, *J. Res. Natl. Bur. Stand. Sect. C* **71**, 299 (1967).
6. R. Apfel, *J. Acoust. Soc. Am.* **49**, 145 (1971).
7. _____ and M. Smith, *J. Appl. Phys.* **48**, 2077 (1977).
8. S. Henderson and R. J. Speedy, *J. Phys. E* **13**, 778 (1980); *J. Phys. Chem.* **91**, 778 (1980).
9. J. C. Fisher, *J. Appl. Phys.* **19**, 1063 (1948).
10. M. Blander and J. Katz, *Am. Inst. Chem. Eng. J.* **21**, 833 (1975).
11. D. H. Trevena, *Contemp. Phys.* **17**, 109 (1976); *Am. J. Phys.* **47**, 341 (1979); *Cavitation and Tension in Liquids* (Adam Hilger, Bristol, England, 1987); S. W. Benson and E. Gerjuoy, *J. Chem. Phys.* **17**, 914 (1949); A. Saul and W. Wagner, *J. Phys. Chem. Ref. Data* **18**, 1537 (1989).
12. R. J. Speedy, *J. Phys. Chem.* **86**, 982 (1982).
13. E. Roedder, *Science* **155**, 1413 (1967).
14. J. L. Green, D. J. Durben, G. H. Wolf, C. A. Angell, *ibid.* **249**, 649 (1990).
15. S. M. Sternar and R. J. Bodnar, *Geochim. Cosmochim. Acta* **48**, 2659 (1984).
16. M. Rovetta, personal communication.
17. The Raman spectra were obtained with a triple spectrometer (Instruments S.A. S3000) equipped with a multichannel diode array detector (Princeton Instruments IY-750). Raman scattering was excited with the 488-nm line of an Ar^+ laser that was focused to a small spot (~5 μm) in the inclusion. Power levels at the inclusion were less than 10 mW. The VV polarized Raman scattered light was collected in a 180° backscattering geometry. To minimize birefringence effects, we oriented the sample such that the laser beam and collection optical axis were collinear with the *c* axis of the quartz host.
18. From data on the expansivity and compressibility of quartz and the compressibility of water we can calculate that the largest pressure correction needed for the matrix compliance effect will be 13% (at the maximum tension) and it falls rapidly at higher temperature.
19. L. Haar, J. Gallagher, G. S. Kell, *National Bureau of Standards-National Research Council Steam Tables* (McGraw-Hill, New York, 1985). See also C. A. Angell, W. J. Sichina, M. Oguni, *J. Phys. Chem.* **86**, 998 (1982).
20. A. Geiger, P. Mausbach, J. Schnitker, in *Water and Aqueous Solutions*, G. W. Neilson and J. Enderby, Eds. (Adam Higler, Bristol, England 1986), pp. 15–30; A. Geiger, in *Correlations and Connectivity*, H. E. Stanley and N. Ostrowsky, Eds. (Kluwer Academic, Dordrecht, 1990), p. 198.
21. D. W. Oxtoby, *J. Chem. Phys.* **89**, 7521 (1988).
22. J. L. Katz, personal communication.
23. V. P. Skripov, in *Water and Steam*, J. Straub and K. Scheffler, Eds. (Pergamon, Elmsford, NY, 1980).
24. N. B. Vargaftik, B. N. Volkov, L. D. Voljak, *J. Phys. Chem. Ref. Data* **12**, 817 (1983).
25. C. A. Angell, *Annu. Rev. Phys. Chem.* **34**, 593 (1983).

26. This work was supported by the National Science Foundation (grants NSF-DMR CHE8304887 and NSF-EAR8657437) and the Shell Fellowship Foundation. We are grateful to J. Holloway for allowing us the use of his high-pressure annealing facility and for advice.

2 May 1991; accepted 8 August 1991

Ice Flexure Forced by Internal Wave Packets in the Arctic Ocean

PETER V. CZIPOTT, MURRAY D. LEVINE, CLAYTON A. PAULSON, DIMITRIS MENEMENLIS, DAVID M. FARMER, ROBIN G. WILLIAMS

Tiltmeters on the Arctic Ocean were used to measure flexure of the ice forced by an energetic packet of internal waves riding the crest of diurnal internal bores emanating from the Yermak Plateau, north of the Svalbard Archipelago. The waves forced an oscillatory excursion of 36 microradians in tilt of the ice, corresponding to an excursion of 16 micrometers per second in vertical velocity at the surface and of 3.5 millimeters in surface displacement. Strainmeters embedded in the ice measured an excursion of 3×10^{-7} in strain, consistent with ice flexure rather than compression. The measured tilt is consistent with direct measurements of excursions in horizontal current near the surface (12 centimeters per second) and in vertical displacement (36 meters) of the pycnocline 100 meters below the surface.

INTERNAL GRAVITY WAVES IN THE world's oceans are important in transporting momentum and energy both horizontally and vertically. The wave field is remarkably constant in space and time, permitting the formulation of a "universal" statistical description (*1*), yet the processes that generate and dissipate these waves are not well understood. However, internal waves in the Arctic Ocean appear to be more variable than waves in other oceans (*2*) and hence may allow study of specific mechanisms of wave growth, propagation, and decay. Measurement of ice tilt is a simple way to observe internal waves from the surface of the Arctic Ocean.

Internal waves generate large displacements of water deep in the ocean. Vertical displacements at the surface are orders of magnitude smaller and masked by noise from turbulence and wind waves on open seas. In most internal wave models, such surface displacements are ignored and a rigid-lid boundary condition is invoked in which the vertical displacement of the sea surface is set to zero (*3*). The ice cover of the Arctic Ocean suppresses surface wave noise and enables direct measurement of vertical displacements of the surface forced by internal waves.

In this report, we describe coherent measurements of ice tilt forced by internal waves in the Arctic Ocean. Observations were made at the oceanography ice camp of the Coordinated Eastern Arctic Experiment (CEAREX) as it drifted over the northern flank of the Yermak Plateau (*4*). Three electrolytic bubble level tiltmeters (*5*) (Fig. 1) were frozen to the surface of the ice in a triangular array. One axis of each meter pointed north and the other east. Three triaxial strainmeters (*6*), with one arm of each meter pointing north, formed another array. We also measured vertical velocity and temperature in the pycnocline using an acoustic Doppler current profiler (ADCP) (*7*) and temperature sensors (*8*) moored near the center of the tilt and strain arrays. Three additional temperature sensors at a depth of 99.5 m formed a triangular moored array. Horizontal water velocity near the surface was measured with a triangular array of acoustic transmitters and receivers (*9*) centered about 337 m to the south of the ADCP mooring.

An internal wave packet was observed passing the ice camp at 82.53°N, 8.58°E between 00 and 02 hours universal time coordinated (UTC) on 18 April 1989 (Fig. 2) (*10*). The wave forced a peak-to-peak ice tilt of 36 μrad (*11*) in a north-south (N-S) direction, in phase with the vertical component of seawater velocity in the pycnocline (*12*) extending from about 100 to 200 m in water 1800 m deep. The vertical velocity in the packet had a maximum excursion of 15 cm/s at a depth near 125 m. Water temperature also revealed vertical displacement in a

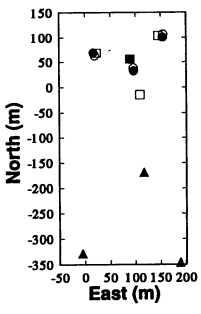

Fig. 1. Instrumentation layout at the CEAREX oceanography ice camp. Solid circles, tiltmeter array; open circles, strainmeter array; solid square, central mooring with ADCP and temperature meters; open squares, satellite moorings with temperature meters; solid triangles, vertices of the horizontal, path-averaging acoustic current meter. Coordinate orientation is aligned with true north for 18 April 1989.

P. V. Czipott, SQM Technology, Inc., Post Office Box 2225, La Jolla, CA 92038.
M. D. Levine and C. A. Paulson, College of Oceanography, Oregon State University, Oceanography Administration Building 104, Corvallis, OR 97331.
D. Menemenlis and D. M. Farmer, Institute of Ocean Sciences, Post Office Box 6000, Sidney, British Columbia, Canada V8L 4B2.
R. G. Williams, Department of Oceanography, U.S. Naval Academy, Annapolis, MD 21402.

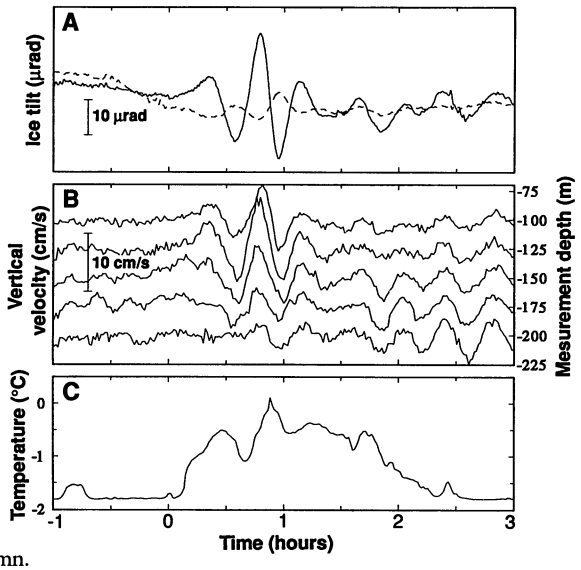

Fig. 2. Signals during passage of a packet of internal waves between 00 and 02 hours UTC on 18 April 1989 (Julian day 108). (**A**) Ice tilt measured in an N-S direction (solid line) and in an E-W direction (dashed line) (*27*). The packet produced a maximum excursion of 36 μrad in N-S tilt and 7 μrad in E-W tilt. (**B**) Vertical velocity measured at depths of 100, 125, 150, 175, and 200 m, as marked on the right ordinate. The maximum excursion of vertical velocity in the packet was 15 cm/s at 125 m. (**C**) Water temperature at a depth of 99.5 m. Before the arrival of the packet, the thermometer was in a nearly isothermal mixed layer and was insensitive to vertical displacement of water. The mixed layer shoaled as the packet arrived. The thermometer, then in a thermocline, responded to displacements of the water column.

signal 90° out of phase with tilt and vertical velocity. Tiltmeter and temperature arrays showed that the packet propagated in a direction within 20° of true north at a speed of 0.45 m/s; its wavelength was 632 m and its period was 24 min (*13*). The comparatively small east-west (E-W) tilt shows that wave crests were orthogonal to the propagation vector. The wave form preserved its shape as it propagated through the instrument arrays.

For a coherent wave form with long crests moving horizontally at speed c along characteristics specified by $x - ct = \xi$, the surface displacement $\eta(\xi)$ depends on ξ alone. Vertical velocity of the surface (*14*), $u_z = \partial\eta/\partial t$, is then proportional to its tilt, $\tau_x = \partial\eta/\partial x$, because $u_z = -c\partial\eta/\partial\xi = -c\tau_x$. For $c = 0.45$ m/s, a peak tilt of 36 μrad corresponds to a peak vertical velocity of the surface of 16 μm/s (Fig. 3). The vertical velocity at the surface was opposite in phase to vertical velocity in the pycnocline, in keeping with displacements expected from waves on an interface between two fluid layers (*15*). Conventional current meter measurements of water velocity near the surface did not detect the small velocities forced by internal waves, because flow over the rough bottom of the ice leads to turbulence (*16*). The ice acts as a spatial filter to suppress small-scale turbulence and enables tiltmeters to measure vertical surface currents from internal waves.

To relate tilt to horizontal velocity near the surface, we used Bernoulli's relation (*17*) in linear form for potential flow at the surface

$$\rho g\eta = \rho(\partial\phi/\partial t)_o - \delta P \qquad (1)$$

where ρ is the density of seawater in the mixed layer, $g = 9.8$ m/s^2, and $(\partial\phi/\partial t)_o$ is the rate of change of the velocity potential ϕ at the surface. Ice flexure supports a pressure differential δP at the interface of ice and water. For internal waves at wavelengths λ appreciably greater than the thickness h of the ice ($h/\lambda < 10^{-2}$), δP is negligible and the ice is a flaccid membrane that responds to wave forcing as a free surface (*18*). Ice tilt is then proportional to horizontal acceleration of seawater at the surface

$$\tau = -(1/g)(\partial \mathbf{u}_h/\partial t)_o \qquad (2)$$

where the relations $\tau = \nabla_h\eta$ and $\mathbf{u}_h = -\nabla_h\phi$ express tilt τ and horizontal velocity at the surface $\mathbf{u}_h$ as horizontal gradients of surface displacement and velocity potential, respectively. The horizontal velocity at the surface, determined by numerical integration over time of surface tilt, is approximately in phase with horizontal velocity measured directly by the acoustic array at a depth of 8 m, but is two-thirds of its amplitude (Fig. 3). We attribute the discrepancy to the Doppler shift introduced by a steady ice camp drift of 7.5 cm/s and to nonlinear terms in Bernoulli's relation, which we have neglected in the first-order analysis presented here. Each of these factors accounts for an error of roughly 15%.

Equation 2 shows that tilt of the ice reflects horizontal acceleration at the surface. In addition, the kinematics of surface displacement implies that the rate of change of tilt is the horizontal gradient of vertical velocity at the surface: $\partial\tau/\partial t = (\nabla_h u_z)_o$ Neither a steady flow nor a spatially uniform flow forces tilt of the ice cover.

Compatibility of these two relations specifies polarization of velocity at the surface, namely, $(\partial^2 u_h/\partial t^2)_o = -g(\nabla_h u_z)_o$. For long wave crests progressing horizontally at frequency ω and wave number k, vertical and horizontal velocities will be 90° out of phase and the ratio of vertical to horizontal velocity will be ω^2/gk. For the observed period and wavelength of the wave packet, the predicted velocity ratio is 2×10^{-4}. The ratio of vertical velocity (16 μm/s) to horizontal velocity (8 cm/s), inferred from measured ice tilt forced by the packet, agrees with this predicted value.

Polarization of velocity at the surface determined from measurements of tilt also agrees with the value expected (*19*) for dispersion of interfacial waves on a sharp pycnocline at a depth of 115 m, marking a density contrast of 0.39 kg/m^3. The time integral of surface vertical velocity gives surface displacement. We determined surface displacement in two ways: (i) by numerical integration of vertical velocity at the surface inferred from tilt (from Fig. 3), and (ii) by numerical integration of vertical velocity in the pycnocline (from Fig. 2), scaled by the ratio of surface displacement to pycnocline displacement expected in a two-layer fluid.

To find surface displacement from displacement of the pycnocline, we supposed that the integral over time of vertical velocity in the pycnocline gives displacement of the interface between the mixed layer and the water below (*20*). For two fluid layers covered by a sheet of ice, the expression (*21*)

$$\frac{\eta}{\zeta} \approx \frac{-(\delta\rho/\rho)e^{-kd}}{1 + \mathcal{R}} \qquad (3)$$

gives the ratio of surface displacement η to

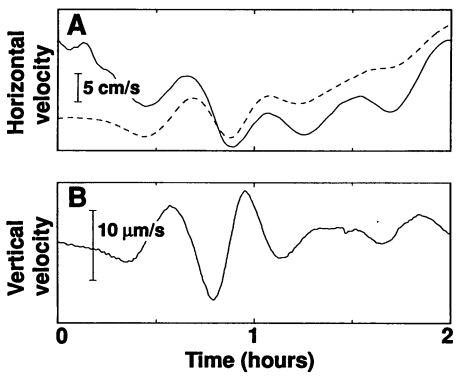

Fig. 3. Horizontal and vertical seawater velocity near the surface during the internal wave packet. (**A**) N-S horizontal current, measured at a depth of 8 m by the path-averaging acoustic current meter (solid line), showed a maximum excursion of 12 cm/s during the packet, with a phase shift of 95°±13° from ice tilt (Fig. 2) (*28*). Horizontal current at the surface, inferred from N-S tilt using Eq. 2 (dashed line), shows a maximum excursion of 8 cm/s during the packet and is in phase with current measured directly. (**B**) Vertical velocity of the ocean surface inferred from N-S tilt for a coherent wave form propagating at $c = 0.45$ m/s. The maximum excursion in surface velocity is 16 μm/s. No other instrument measured vertical velocity of the surface with such resolution of internal waves.

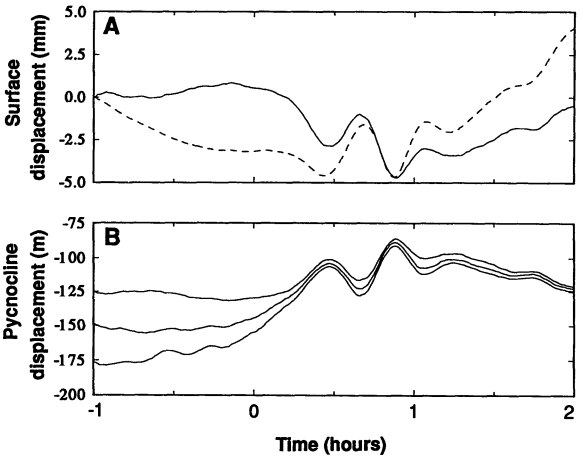

Fig. 4. Comparison of surface and pycnocline displacements forced by the internal wave packet. (**A**) Surface displacement determined by numerical integration over time of N-S ice tilt, scaled by $-c$ (dashed line), and surface displacement determined by numerical integration of vertical velocity in the pycnocline at a depth of 125 m, scaled by Eq. 3 (solid line). The lines start from zero displacement at −1 hours UTC and overlap during passage of the packet, each showing a peak excursion of about 3.5 mm. (**B**) Pycnocline displacement determined by numerical integration over time of vertical velocity in the pycnocline, starting at 125-, 150-, and 175-m depths. It shows a peak excursion of 36 m during passage of the packet.

displacement of the pycnocline ζ by a progressive wave with wave number k. The density contrast across the pycnocline is $\delta\rho$, and ρ is density of a mixed layer of depth d. Rigidity $\mathcal{R}$ of the ice cover is negligible for $hk \ll 1$ (*18*).

The two methods of estimating surface displacement agree during passage of the wave packet (Fig. 4); thus, the packet held its wave form as it propagated over a distance of one wavelength. It forced an excursion of 3.5 mm in surface displacement.

Numerical integration of vertical velocity in the pycnocline shows that its maximum excursion was about 36 m during passage of the packet. The packet rode an undulant bore that displaced the pycnocline upward by about 15 m. Integrated velocity compares closely with pycnocline displacement determined from the temperature record of Fig. 2. We used a mean gradient of −31 m/°C in the thermocline (*22*) to convert temperature to a measure of displacement also indicating a peak excursion of 36 m.

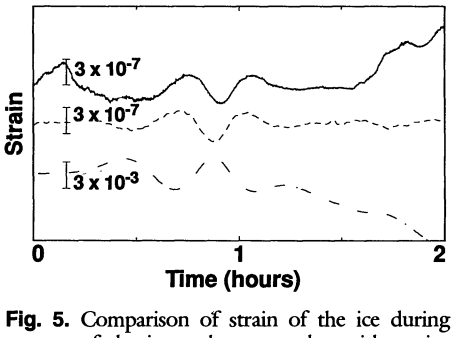

Fig. 5. Comparison of strain of the ice during passage of the internal wave packet with strains inferred from ice tilt. Longitudinal strain (solid line) measured along an N-S axis on the surface of the ice showed an excursion of 3×10^{-7} in strain, coming from the packet. Flexural strain (dashed line), inferred from measured tilt using Eq. 5 with $h = 2$ m, is in phase and commensurate with measured strain. Compressional strain (dot-dashed line), inferred from measured tilt using Eq. 4 with $h = 2$ m, shows an excursion of 3×10^{-3} that is opposite in phase and four orders of magnitude larger than measured strain.

Strain in the ice from wave motion below it comes mainly from bending instead of longitudinal compression of the ice. For ice compression (*23*), longitudinal strain in the direction of propagation, e_{xx}, is proportional to an integral of ice tilt in the same direction

$$e_{xx} = \frac{-2(1-\nu)}{h\nu}\int \tau_x\,dx = \frac{2c(1-\nu)}{h\nu}\int \tau_x dt \qquad (4)$$

where ν is Poisson's ratio and $\xi = x - ct$ relates integrals over space and time. For ice flexure (*24*), strain is proportional to derivatives of tilt

$$e_{xx} = \frac{-h}{2}\frac{\partial \tau_x}{\partial x} = \frac{h}{2c}\frac{\partial \tau_x}{\partial t} \qquad (5)$$

Strain of the ice, measured along an N-S direction, showed an excursion of 3×10^{-7} during passage of the wave packet (Fig. 5). The comparison of measured strain to compressional and flexural strain inferred from measured ice tilt (Fig. 5) demonstrates that strain and tilt forced by coherent internal waves below the ice come mainly from flexure of the ice cover with little or no direct compression.

Tiltmeters are a valuable tool for oceanography of polar seas. They give a measure of velocity at the surface that no other instrument can provide (*25*). Because they are easy to deploy on the ice, arrays of autonomous tiltmeters can monitor arctic flow on the scale of internal waves over wide areas in all seasons. They offer a remarkable capability for monitoring surface displacements of the Arctic Ocean.

REFERENCES AND NOTES

1. C. J. R. Garrett and W. H. Munk, *Geophys. Astrophys. Fluid Dyn.* **2**, 255 (1972); *J. Geophys. Res.* **80**, 291 (1975).
2. M. D. Levine, C. A. Paulson, J. H. Morison, *J. Geophys. Res.* **92**, 779 (1987); M. D. Levine, *ibid.* **95**, 7347 (1990).
3. A. E. Gill, *Atmosphere-Ocean Dynamics* (Academic Press, San Diego, 1982), p. 127.
4. During its operation from 26 March to 30 April 1989, the CEAREX oceanography camp drifted from 83.25°N, 10.28°E, over the deep water (4000 m) of the Nansen Basin, to 82.08°N, 5.03°E, over the northern slope of the Yermak Plateau. For a map of camp drift, see L. Padman and T. M. Dillon [*J. Geophys. Res.* **96**, 4769 (1991)].
5. We fielded one tiltmeter with a rated resolution of 0.1 μrad (Applied Geomechanics, Inc., Santa Cruz, CA) and two tiltmeters rated at 0.005 μrad (Rockwell International, Autonetics Division, Anaheim, CA). Tilt time series come from data recorded once per second, through a 250-mHz antialiasing filter. Time series of ice tilt shown here were digitally filtered at 10 mHz to suppress oscillations from long-period swell.
6. V. A. Squire, *J. Glaciol.* **20**, 425 (1978); R. G. Williams, N. R. Davis, S. C. Moore, *Polar Rec.* **26**, 203 (1990). Time series of ice strain come from data recorded on 14-track analog tape; these data were then filtered and digitized at 1-s intervals. Strain sensitivity exceeds 10^{-8}.
7. ACDP from RD Instruments, Inc., San Diego, CA. The sonar pings at about 1-s intervals. Returns were averaged for 1 min, then digitally stored. Current sensitivity approaches 1 cm/s.
8. Temperature sensors from SeaBird Electronics, Inc., Bellevue, WA. Temperature was sampled at 1-s intervals and averaged for 1 min, giving a sensitivity of 1 mK.
9. D. Menemenlis and D. M. Farmer, in preparation. Differences in travel time of pulses transmitted between each vertex of the array give horizontal current over each leg. Averaging horizontal velocity, sampled at 0.91-s intervals, for 1 min gives a sensitivity near 0.1 mm/s.
10. As the camp drifted near the 2000-m isobath along the northern slope of the Yermak Plateau, from 13 April to 20 April, strong internal bores passed diurnally. Internal wave packets, with two to three oscillations at periods from 20 to 40 min, rode the bores. The packet described herein passed at constant speed without change of form. Over the limited aperture (~1 km) of measurement arrays at the camp, it resembled a solitary wave coming from tidal flow over the Yermak Plateau [L. A. Ostrovsky and Yu. A. Stepanyants, *Rev. Geophys.* **27**, 293 (1989)].
11. Ambient noise from incoherent internal waves is a few tenths of a microradian.
12. The mean mixed layer [$\sigma_t = 27.47$, with density $\rho = 1 + \sigma_t(10^{-3})$ in grams per cubic centimeter] extends to a depth of about 115 m when undisturbed. Density increases nearly linearly thereafter to $\sigma_t = 27.86$ at 200 m, after which it increases slowly to $\sigma_t = 27.98$ at 600 m. [J. Morison and R. Andersen, unpublished technical report (Polar Science Center, University of Washington, Seattle, WA).]
13. Propagation direction, wave speed and wavelength were determined by measurement of time lags as the packet passed through a sensor array. The parameters measured by the tiltmeter array agreed within about 5% with results from the temperature array.
14. Vertical velocity, u_z, of a particle on a surface is the material derivative of surface displacement, η; that is, $u_z = \partial\eta/\partial t + \mathbf{u}_h \cdot \boldsymbol{\tau}$, where $\boldsymbol{\tau} \equiv \nabla_h\eta$ is tilt of the surface and $\mathbf{u}_h$ is horizontal velocity at the surface [J. J. Stoker, *Water Waves* (Interscience, New York, 1957), pp. 11 and 21]. We used the linear approximation $u_z \approx \partial\eta/\partial t$, which is adequate for a first-order analysis.
15. J. R. Apel, *Principles of Ocean Physics* (Academic Press, San Diego, 1987), p. 236.
16. M. G. McPhee, in *Deep Convection and Deep Water Formation*, J.-C. Gascard and P.-C. Chu, Eds. (Elsevier, New York, in press).
17. B. Kinsman, *Wind Waves* (Prentice-Hall, Princeton, 1965), p. 112.
18. For a thin plate of thickness h and density ρ_i floating on water of density ρ, the expression [(*26*), p. 280]

$$\delta P = \left[\mathcal{R} - \left(\frac{\omega^2}{gk}\right)\left(\frac{\rho_i}{\rho}\right)kh\right]\rho g\eta$$

gives the pressure differential from an oscillation at frequency ω and wave number k, where the relation

$$\mathcal{R} = \frac{E(hk)^4}{12(1-\nu^2)\rho g h}$$

gives the rigidity of the ice, $\mathcal{R}$. Values for the elastic modulus of ice, E, and Poisson's ratio, ν, are 9.2×10^9 Pa and 0.365, respectively [M. Ewing, A. P. Crary, A. M. Thorne, Jr., *Physics (N.Y.)* **5**, 165 (1934)]. For ice 1 m thick, $\mathcal{R} \approx (hk)^4 \times 10^5$, so rigidity of the ice is negligible at wavelengths of several hundred meters ($hk < 10^{-2}$). Differential pressure is then negligible compared to hydrostatic pressure from surface displacement.

19. The expression (*21*) $\omega^2/gk = (\delta\rho/\rho)(1 - e^{-2kd})/2$ gives the dispersion of waves at frequency ω and wave number k propagating on a sharp pycnocline at depth d with a density contrast $\delta\rho$.
20. One must use coordinates fixed to isopycnal surfaces in the integration of u_z [R. Pinkel, J. A. Smith, J. T. Sherman, S. A. Anderson, *J. Phys. Oceanogr.* **21**, 527 (1991)]. The ADCP, with a vertical binning of 4 m, allowed us to approximate the coordinates by using the value of u_z at the current value of depth in the running integral.
21. M. Ewing and A. P. Crary, *Physics (N.Y.)* **5**, 181 (1934).
22. A linear approximation of the temperature gradient in the pycnocline measured by conductivity-temperature-depth casts during the bore [L. Padman and T. M. Dillon, *Data Report 150, Ref. 90-2* (Oregon State University, Corvallis, 1990), p. 135] gives $\partial z/\partial T \approx -31.1$ m/°C.
23. H. Kolsky, *Stress Waves in Solids* (Dover, New York, 1963), p. 79.
24. For flexural waves in a thin plate ($hk \ll 1$), surface tilt is given by the expression [(*26*), p. 277] $\mathbf{d}_h = -(h/2)\boldsymbol{\tau}$, where $\mathbf{d}_h$ is horizontal displacement at the surface.
25. Strains from nondeviatoric compression dominated strainmeter records at internal wave frequencies and had amplitudes of many times 10^{-7}. They arose from ice deformation driven over large spatial scales and usually obscured the local signal from internal waves. Only two of the nine strainmeter axes revealed the energetic internal wave packet. The measurements showed that the packet locally forced bending instead of nondeviatoric compression, contrary to earlier speculation [T. O. Manley *et al.*, *Eos* **63**, 627 (1982)].
26. C. Wang, *Applied Elasticity* (McGraw-Hill, New York, 1953).
27. Our coordinate convention defines a right-handed system with the x-axis positive northward, the y-axis positive westward, and the z-axis positive upward. We define tilt as the positive gradient of vertical displacement and strain as positive for extension.
28. The phase shift relates horizontal velocity to tilt at the same location. Horizontal velocity was actually measured 337 m south of the tiltmeter. Using the wave speed and propagation direction, we shifted the time coordinate of horizontal velocity to represent velocity at the tiltmeter.
29. The Office of Naval Research (ONR) Arctic Program, directed by T. B. Curtin, supported CEAREX operations and the work of individual authors. P.V.C. acknowledges support for the ice camp experiment from the Office of Naval Technology, monitored by ONR under contract N00014-89-C-0087. Data analysis was supported by ONR contract N00014-90-C-0140. The work of M.D.L. and C.A.P. was supported by ONR contract N00014-87-K-0009 and grant N00014-90-J-1048, that of D.M. and D.M.F. by grant N00014-88-J-1102, and that of R.G.W. by grants N00014-86-G-0024 and N00014-90-J-1390. We thank J. H. Morison, chief scientist of the ice camp science program. M.D.L. and C.A.P. thank J. Simpkins, D.M. and D.M.F. thank R. Teichrob, and R.G.W. thanks S. C. Moore for assistance at the camp. N. Davis digitized the strainmeter records for this work. We thank the other scientists at the camp for helpful discussions and D. Horn and the crew from the Polar Science Center, University of Washington, led by A. Heiberg and camp manager M. Welch, for vital logistic support.

22 May 1991; accepted 31 July 1991

Sudden Extinction of the Dinosaurs: Latest Cretaceous, Upper Great Plains, U.S.A.

PETER M. SHEEHAN, DAVID E. FASTOVSKY, RAYMOND G. HOFFMANN, CLAUDIA B. BERGHAUS,* DIANE L. GABRIEL†

Results of a three-year field study of family-level patterns of ecological diversity of dinosaurs in the Hell Creek Formation of Montana and North Dakota show no evidence (probability $P < 0.05$) of a gradual decline of dinosaurs at the end of the Cretaceous. Stratigraphic reliability was maintained through a tripartite division of the Hell Creek, and preservational biases were corrected for by comparison of results only from similar facies as well as through the use of large-scale, statistically rigorous survey and collection procedures. The findings are in agreement with an abrupt extinction event such as one caused by an asteroid impact.

THE CAUSE OF EXTINCTION OF DINOSAUR faunas at the end of the Mesozoic era remains controversial. Two principal endmember hypotheses have been developed. One is that dinosaur populations dwindled gradually at the end of the Cretaceous, probably as a result of climatic changes (*1–3*). The other is that an asteroid impact produced sudden environmental changes that caused an abrupt extinction (*4, 5*). Resolution of the mechanism responsible for the extinction requires knowledge of changes in dinosaur populations immediately before and at the end of the Cretaceous. Earlier field studies, however, were not designed to examine patterns of dinosaur diversity during this interval in a statistically meaningful fashion (*6*). We therefore undertook a 3-year study in which dinosaur fossils were sampled through the Hell Creek Formation, a unit that represents the last 2 to 3 million years of the Cretaceous Period (7) in the upper Great Plains of the United States (Fig. 1). Patterns of family-level dinosaur ecological diversity are used to assess the general robustness of dinosaur populations.

Several considerations hinder analysis of the extinction in the Hell Creek. The Hell Creek has complex, laterally discontinuous facies that make biostratigraphic distributions difficult to determine. Fossils are found in interfingering channel and floodplain deposits that reflect the repeated erosion of floodplains by ancient meandering streams. Superimposed soils were formed during potentially long intervals of nondeposition. Correlation of beds across tens of meters is often impossible because of such complexity (*8, 9*). For example, a stream meandering over a floodplain can erode a broad channel that is later filled by much younger deposits. As a result, sediments at approximately the same topographic level can be of quite different ages because of channel erosion and infilling by younger sediments. Moreover, equivalent thicknesses of floodplain and channel sediments cannot easily be compared, because the former took orders of magnitude more time to be deposited than the latter (*7–10*).

Detailed correlations are tenuous beyond a limited area, even though broad areas must be searched to find significant numbers of fossils. To overcome the problems of the lateral nonpersistence of strata and differing sedimentation rates, we divided the Hell Creek Formation into three approximately equal, successive intervals, against which dinosaur ecological diversity could be measured. The top of the upper stratigraphic interval was the boundary clay (commonly associated with coal) containing the iridium anomaly (*11*). No dinosaur bones were found above this layer, and the closest dinosaur specimen was found 60 cm below it. The lower stratigraphic boundary was established at the lithostratigraphic contact between the terrestrial Hell Creek and underlying, marginal-marine Fox Hills Sandstone, which contains no dinosaurs. Because the upper boundary is approximately isochronous and the Hell Creek Formation is 70 to 90 m thick in all of the study areas, it is reasonable to infer that crude correlations can be made between equivalent, measured

P. M. Sheehan, C. B. Berghaus, D. L. Gabriel, Department of Geology, Milwaukee Public Museum, Milwaukee, WI 53233.
D. E. Fastovsky, Department of Geology, University of Rhode Island, Kingston, RI 02881.
R. G. Hoffmann, Division of Biostatistics, Medical College of Wisconsin, Milwaukee, WI 53226.

*Present address: School of Veterinary Science, Department of Surgical Sciences, University of Wisconsin, Madison, WI 53706.
†Present address: Department of Paleontology, Museum of the Rockies, Montana State University, Bozeman, MT 59717.